Oversampled A/D Conversion and Error-Rate Dependence of Non-Bandlimited Signals with Finite Rate of Innovation

Ivana Jovanović, Baltasar Beferull-Lozano, *Associate Member, IEEE*

Abstract

We study the problem of A/D conversion and error-rate dependence of a class of non-bandlimited signals which have a finite rate of innovation, particularly, a continuous periodic stream of Diracs, characterized by a finite set of time positions and weights. Previous research has only considered sampling of this type of signals, ignoring the presence of quantization, which is necessary for any practical application. We first define the concept of consistent reconstruction for these signals and introduce the operations of both: a) oversampling in frequency, determined by the bandwidth of the lowpass filter used in the signal acquisition, and b) oversampling in time, determined by the number of samples in time taken from the filtered signal. Accuracy in a consistent reconstruction is achieved by enforcing the reconstructed signal to satisfy three sets of constraints, defined by: the low-pass filtering operation, the quantization operation itself and the signal space of continuous periodic streams of Diracs. We provide two schemes to reconstruct the signal. For the first one, we prove that the mean squared error (MSE) of the time positions is of the order of $O(1/R_t^2 R_f^3)$, where R_t and R_f are the oversampling ratios in time and in frequency, respectively. For the second scheme, which has a higher complexity, it is experimentally observed that the MSE of the time positions is of the order of $O(1/R_t^2 R_f^5)$. Our experimental results show a clear advantage of consistent reconstruction over non-consistent reconstruction. Regarding the rate, we consider a threshold crossing based scheme where, as opposed to previous research, both oversampling

The work presented in this paper was supported (in part) by the National Competence Center in Research on Mobile Information and Communications Systems (NCCR-MICS), a center supported by the Swiss National Science Foundation under grant number 5005-67322. The material in this paper was presented in part at the IEEE International Conference on Acoustics, Speech and Signal Processing, 2004, Montreal and IEEE International Symposium on Information Theory, 2004, Chicago.

Ivana Jovanović and Baltasar Beferull-Lozano are with Swiss Federal Institute of Technology-EPFL, IC-LCAV, CH-1015 Lausanne, Switzerland (e-mail:ivana.jovanovic@epfl.ch, baltasar.beferull@epfl.ch, fax: (+41 21) 693 4312, tel: (+41 21) 693 1271).

in time and also in frequency influence the coding rate. We compare the error-rate dependence behavior that is obtained from both increasing the oversampling in time and in frequency, on the one hand, and on the other hand, from decreasing the quantization stepsize.

Index Terms

Finite rate of innovation, quantization, oversampling, consistency, projection, convexity, threshold crossing encoding.

I. INTRODUCTION

Recent results in sampling theory [1] have shown that it is possible to develop exact sampling schemes for a certain set of non-bandlimited signals, characterized by having a finite number of degrees of freedom per unit time, which is called finite rate of innovation. Taking a finite number of uniform samples, obtained from an appropriate sampling kernel, we are able to achieve perfect reconstruction. Some of these signals with finite rate of innovation, such as streams of Diracs, have found several applications in CDMA [2], UWB [3] and sensor field sampling [4]. For example, results in [1] can be applied to the problem of multipath delay estimation in wideband channels. On the other hand, in the context of sensor networks measuring physical phenomena, such as temperature, local heat sources can be well modeled by Diracs and the sampling kernel in this case is given by the Green's function of the heat diffusion equation [5]. In [1], [2], [3], it was assumed that we have no quantization of the acquired samples. However, in any practical application quantization is required. An irreversible loss of information, introduced by quantization makes perfect reconstruction no longer possible. Motivated by the need of quantization, we investigate Analog-to-Digital (A/D) conversion and the error-rate dependence of non-bandlimited signals with finite rate of innovation, which has not been considered in previous research.

In this paper, we focus on the A/D conversion of a particular class of signals with finite rate of innovation, namely, continuous periodic stream of K Diracs, characterized by a set of time positions $\{t_k\}_{k=0}^{K-1}$ and weights $\{c_k\}_{k=0}^{K-1}$. We study the reconstruction quality of time positions under the presence of quantization. There are two reasons for this: 1) it can be shown that the error in weights depends on the error in time positions, and 2) in many applications, such as UWB and sensor field sampling, the most important information is contained in the positions of pulses.

High reconstruction accuracy in time positions can be achieved by introducing two types of oversampling: 1) oversampling in frequency, determined by the bandwidth extension of the low-pass sampling kernel, and 2) oversampling in time, determined by the number of samples taken from the acquired

filtered signal. Introducing the oversampling is equivalent to introducing a redundancy in the system, which usually reduces the sensitivity to degradations. Although this idea is very intuitive, the question of fully exploiting that redundancy is not always simple. This can be already observed in the case of A/D conversion of bandlimited signals, where the simple linear reconstruction is not optimal, in the sense that the outputs obtained from quantizing the original and the reconstructed signal are not necessarily the same, implying a larger reconstruction error on average. The key idea to achieve high accuracy is to have a reconstruction that is consistent with all the available knowledge about the signal and the acquisition process. Thus, in our work, we use the concept of consistency by enforcing the reconstructed signal to satisfy three sets of constraints which are related to: 1) the sampling kernel, 2) the quantization operation itself and 3) the space of continuous periodic streams of K Diracs. A signal reconstruction satisfying the three sets is said to provide *Strong* consistency while if it satisfies only the first two sets is said to provide *Weak* consistency.

The concept of consistent reconstruction and the corresponding reconstruction accuracy for the case of bandlimited signals has been considered in [6], [7], [8]. However, there are three essential differences with our work: a) we consider the reconstruction accuracy that is related to the non-bandlimited signal; b) we exploit the knowledge about the structure of the non-bandlimited signal; c) we introduce oversampling in frequency in addition to oversampling in time.

In this work, reconstruction algorithms for both *Weak* and *Strong* consistency are proposed. As a quantitative characterization of the reconstruction quality, we consider the mean squared error (MSE) of the time positions and its dependence on the oversampling in time and in frequency. We focus on the MSE related to time positions because, as we show in this paper, the MSE related to the weights of the Diracs depends fundamentally on the MSE of time positions. For the first algorithm, we show both theoretically and experimentally that the MSE performance for the time positions decreases as $O(1/R_t^2 R_f^3)$, where R_t and R_f are the oversampling ratios in time and frequency, respectively. For the second algorithm, which achieves *Strong* consistency but has a higher complexity, we obtain experimentally an MSE performance of the order of $O(1/R_t^2 R_f^5)$ [9]. Both results show a clear outperformance of consistent reconstructions over non-consistent reconstructions.

We also apply encoding schemes and study the scaling laws that can be achieved for the bit rate and the error-rate dependence, depending on the concrete encoding scheme and the reconstruction algorithm. Regarding the rate, we consider two encoding schemes: a threshold crossing (TC) based scheme, similar to the one proposed in [10] and a PCM encoding scheme, and compare the error-rate dependence that is obtained from both increasing the oversamplings in time and in frequency, on the one hand, and on the

other hand, from decreasing the quantization stepsize. The main novel part of the TC encoding analysis, introduced in our work, is the additional dependence of the maximal number of threshold crossings on the oversampling in frequency, which comes as a consequence of considering non-bandlimited signals with finite rate of innovation. Our results show that, using the TC encoding, we can achieve the same error-rate dependence, for these non-bandlimited signals with finite rate of innovation, by a) increasing the oversampling in time and b) decreasing the quantization stepsize [11]. This is very important from a practical point of view because the cost of halving the quantization stepsize is much higher than that of doubling any of the oversampling ratios (complex and expensive analog circuitry). Moreover, in order to make the TC encoding scheme work in our case, we can adjust three parameters (the quantization stepsize and the two oversamplings), as compared to the case of bandlimited signal [10], where only two parameters are adjusted (the quantization stepsize and the oversampling in time).

Although our theoretical analysis is restricted to periodic streams of Diracs, the algorithms proposed in this paper can be also used for reconstructing other signals with finite rate of innovation such as finite streams of Diracs and nonuniform splines.

This paper is organized as follows. Section II introduces the class of signals given by continuous-time periodic streams of Diracs. Section III defines the oversampling in time and in frequency. Section IV introduces the concept of *Weak* consistency and *Strong* consistency and proposes the corresponding reconstruction algorithms. In Section V, we prove an upper bound for the MSE performance achieved by *Weak* consistency and in Section VI, we present the experimental results for both *Weak* and *Strong* consistency. In Section VII and Section VIII, we describe and analyze the threshold crossing based encoding and address the rate and error-rate dependence. We compare the error-rate dependence as a function of the both oversamplings and the quantization stepsize. Finally, in Section IX, we conclude with a brief summary of our work and directions for future work.

II. Signals with Finite Rate of Innovation

New results on sampling theory show that certain classes of non-bandlimited signals, such as periodic and finite length streams of Diracs, non-uniform splines and piecewise polynomials, can be uniformly sampled with a finite number of samples, using sinc and Gaussian sampling kernels and then perfectly reconstructed. Intuitively, these classes of signals are characterized by having a finite number of degrees of freedom per unit of time, namely, having *a finite rate of innovation*.

In this work, we consider a periodic stream of K Diracs, that is, $x(t) = \sum_{k\in\mathbb{Z}} c_k \delta(t - t_k)$ with period τ, where $t_{k+K} = t_k + \tau$ and $c_{k+K} = c_k$, $\forall k \in \mathbb{Z}$, and $\delta(t)$ denotes a Dirac delta function.

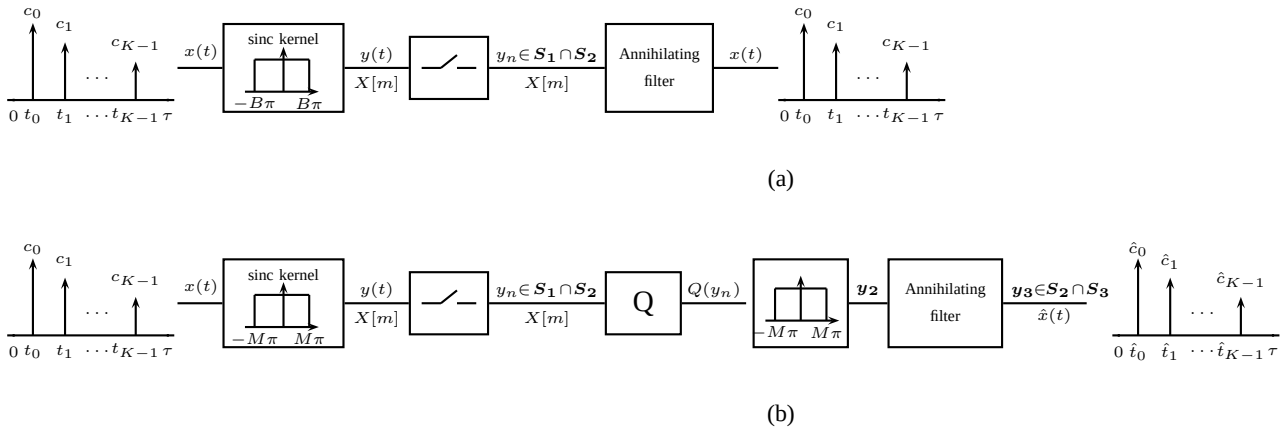

Fig. 1. Reconstruction algorithms for a periodic stream of Diracs: (a) without introducing quantization; (b) introducing quantization of the samples y_n of signal $y(t)$. The annihilating filter in (a) corresponds to the equation (3) and the one in (b) corresponds to the equation (4).

This signal has $\frac{2K}{\tau}$ degrees of freedom per unit of time, since the only knowledge that is required to determine the signal uniquely is given by the K time positions $\{t_k\}_{k=0}^{K-1}$ and the K weights $\{c_k\}_{k=0}^{K-1}$. This signal can be perfectly reconstructed by first applying a sinc sampling kernel $h_B(t) = B\text{sinc}(Bt)$ with bandwidth $[-B\pi, B\pi]$, thus obtaining $y(t) = x(t) * h_B(t)$, and then taking the N uniform samples $\{y_n = y(nT)\}_{n=0}^{N-1}$, where $T = \tau/N$, $B\tau = 2M+1 \geq 2K+1$ and the number of samples is $N \geq 2M+1$. A periodic stream of K Diracs $x(t)$ can be represented through its Fourier series, as follows:

$$x(t) = \sum_{m \in \mathbb{Z}} X[m] e^{j\frac{2\pi m t}{\tau}}, \qquad \text{where } X[m] = \frac{1}{\tau} \sum_{k=0}^{K-1} c_k e^{-j\frac{2\pi m t_k}{\tau}}. \tag{1}$$

After sampling the signal with the sinc sampling kernel, the uniform samples of $y(t)$ are given by:

$$y_n = \sum_{m=-M}^{M} X[m] e^{j\frac{2\pi m n}{N}} \quad \text{where} \quad n = 0, \ldots, N-1. \tag{2}$$

Taking at least $2K+1$ samples $\{y_n\}_{n=1}^{2K+1}$, we can directly from (2) compute the $2K+1$ Fourier coefficients $X[m]$ of the signal $x(t)$. Fourier coefficients $X[m]$ coincides with discrete-time Fourier series[1] (DTFS) of y_n, that is $X[m] = Y[m]$. Having $2K+1$ Fourier coefficients $X[m]$, we can reconstruct first time positions

[1]The definition of DTFS we adopt here is:

$$\text{DTSF}(\{y_n\}_{n=0}^{N-1}) = \{Y[m]\} \quad \text{where} \quad Y[m] = \frac{1}{N} \sum_{n=0}^{N} y_n e^{-j2\pi n m/N}, \quad \text{for} \quad m \in \mathbb{Z}.$$

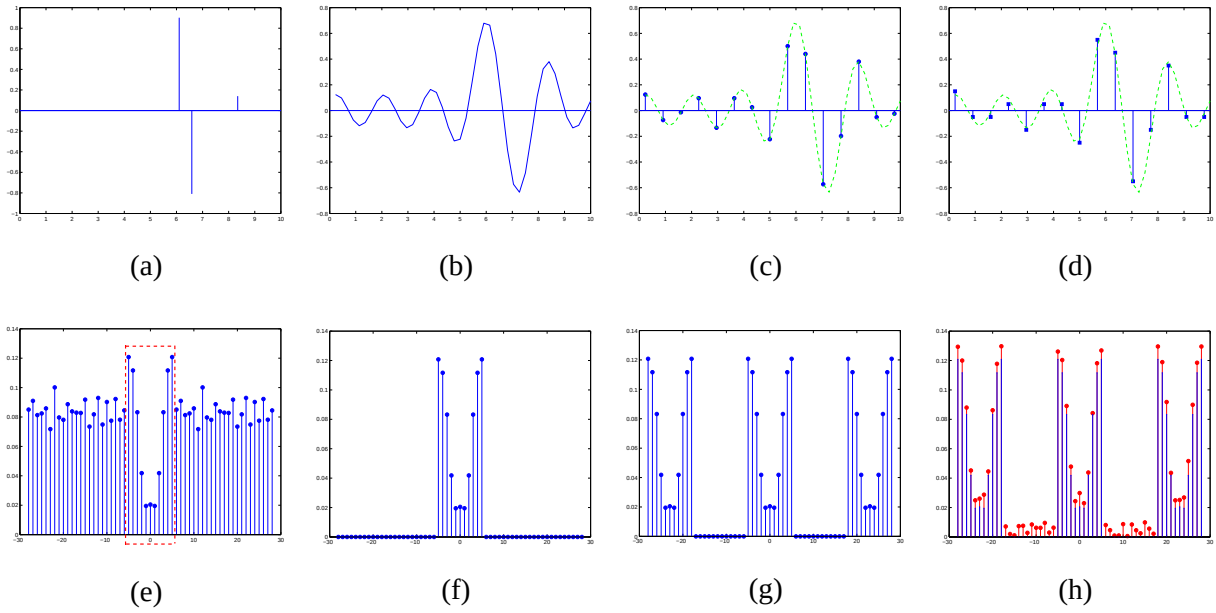

Fig. 2. (a) Original signal $x(t)$ given by a periodic stream of 3 Diracs, $\tau = 10$ and $t_k \in [0, \tau]$, $c_k \in [-1, 1]$; (b) Signal $y(t)$ obtained by filtering $x(t)$ with a sinc sampling kernel; (c) Samples $y_n = y(nT)$; (d) Quantized samples $Q(y_n)$; (e) Fourier coefficients from the stream of 3 Diracs $x(t)$; (f) Fourier coefficients from the signal $y(t)$ that are truncated Fourier coefficients from $x(t)$ and bandlimited to its $2M+1$ central components; (g) N-periodized Fourier coefficients corresponding to DTFS from y_n; (h) DTFS with small error deviations that are added to the Fourier components both in the lowpass region and highpass region, thus making the perfect reconstruction no longer possible.

and then weights. Thus, it is clear that lowpass version of the original signal $x(t)$, that we call $y(t)$, is sufficient for the signal reconstruction. Analyzing the Fourier components in (1), it can be seen that each exponential term $\{u_k = e^{-j\frac{2\pi t_k}{\tau}}\}_{k=0}^{K-1}$ can be annihilated by a first order FIR annihilated filter $A_k(z) = (1 - e^{-j\frac{2\pi t_k}{\tau}} z^{-1})$. Extension of the filter order to K results in a filter $A(z) = \prod_{k=1}^{K}(1 - e^{-j\frac{2\pi t_k}{\tau}} z^{-1})$ that annihilates all Fourier coefficients. In matrix notation, this can be represented as:

$$\begin{pmatrix} X[0] & X[-1] & \dots & X[-K] \\ X[1] & X[0] & \dots & X[-(K-1)] \\ \vdots & \vdots & \ddots & \vdots \\ X[K] & X[K-1] & \dots & X[0] \end{pmatrix} \begin{pmatrix} a_0 \\ a_1 \\ \vdots \\ a_K \end{pmatrix} = \begin{pmatrix} 0 \\ 0 \\ \vdots \\ 0 \end{pmatrix} \tag{3}$$

where a_i is the i-th coefficient of the annihilating polynomial. Thus, if we are given the $2K+1$ exact Fourier coefficients, by setting $a_0 = 1$, we can find the unique solution of (3) that gives all the coefficients of the annihilating filter. The roots of the annihilating filter $A(z)$, $\{u_k = e^{-j\frac{2\pi t_k}{\tau}}\}_{k=0}^{K-1}$, reveal the K time positions $\{t_k\}_{k=0}^{K-1}$, while the corresponding weights $\{c_k\}_{k=0}^{K-1}$ can be then directly computed from (1) (see Fig. 1(a) and Fig. 2).

Notice that all previous steps assume no quantization in amplitude and hence, no error in $\boldsymbol{y} =$

$[y_0, \ldots, y_{N-1}]^T$, which ensures the existence of the previous exact solution. In our work we study A/D conversion for these signals and thus we consider the operation of quantization performed on $\boldsymbol{y}$ (see Fig. 1(b)). The quantization error in amplitude, causes an irreversible loss of information which makes the exact recovery of $x(t)$ no longer possible (see Fig. 2). In order to overcome this problem, as the first step, we are going to introduce the two types of oversampling.

III. Oversampling in Time and Frequency

We consider two types of oversampling in order to compensate the error introduced by quantization. The first one consists of taking more samples $\boldsymbol{y}$ than we need, or equivalently taking samples of $y(t)$ above the Nyquist rate. In that case we have that $N > 2M + 1$. This introduces an *oversampling in time* which is characterized by oversampling ratio $R_t = \frac{N}{2M+1}$.

Notice that we can also perform an additional type of oversampling by extending the bandwidth of the sampling kernel to be greater than the rate of innovation, or equivalently, making $(2M + 1) > (2K + 1)$. We denote this type of oversampling as an *oversampling in frequency* with the oversampling ratio given by $R_f = \frac{2M+1}{2K+1}$. As explained in the following section, the oversampling in frequency will modify the annihilating filter method illustrated in (3), and the corresponding matrix has to be augmented because we use more Fourier coefficients.

We remark also that the number of samples is $N = (2M + 1)R_t = (2K + 1)R_f R_t$, which means that N increases linearly with both types of oversampling. As shown in Sections V and VI, by increasing these two oversamplings, and using proper reconstruction schemes, we can substantially increase the reconstruction accuracy.

IV. Consistent Reconstruction

In the reconstruction process, we enforce the concept of *consistent reconstruction,* previously introduced in [6] for the case of bandlimited signals. The idea of consistent reconstruction is to exploit all the knowledge from both the *a priori* properties of the original signal and the information provided by the quantization process. Thus, the key is to find a reconstruction which is consistent with all the available knowledge. Intuitively, a consistent reconstruction will provide, on average, a better reconstruction accuracy than a non-consistent reconstruction.

We first define all the properties that a reconstruction should satisfy in order to be consistent. Each property defines a set of signals, thus, requiring the satisfaction of a certain property is equivalent to requiring the membership in a certain set of signals. The fact that all properties are satisfied by the

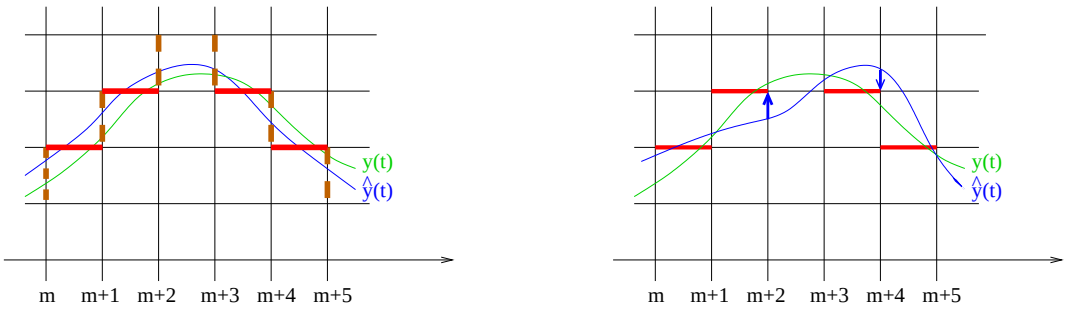

Fig. 3. (a) The estimated function $\hat{y}(t)$ is consistent with the original signal $y(t)$ with respect to the quantization bins. (b) If the estimated function $\hat{y}(t)$ is not consistent with $y(t)$, then we project to the border of the corresponding quantization bin.

original signal ensures that the corresponding sets have a nonempty intersection. All the constraints, or equivalently, the sets, are going to be defined as a subsets of the space of N-periodic discrete-time signals, that we call $\mathcal{H}$.

The first set of constraints $\boldsymbol{S_1}$ is related to the quantization operation. The samples $\boldsymbol{y}$ are quantized by a uniform quantizer[2], that is, $y_n^q = Q(y_n) = \Delta(\lfloor y_n/\Delta \rfloor + 1/2)$ where Δ is the quantization stepsize. Let $l_n = [\Delta\lfloor y_n/\Delta \rfloor, \Delta\lfloor y_n/\Delta \rfloor + \Delta]$ be the quantization interval to which the sample y_n belongs. The sequence $\{y_n^q\}_{n=0}^{N-1}$ gives the information about the intervals in which all the samples lie, namely, $y_n \in l_n$. The set of these intervals is an N-dimensional cube, namely:

Set $\boldsymbol{S_1}$: Given $\boldsymbol{y}$ and $\boldsymbol{y^q} = \mathbb{Q}(\boldsymbol{y}) = [y_0^q, \ldots, y_{N-1}^q]^T$, the set $\boldsymbol{S_1} = \mathbb{Q}^{-1}(\boldsymbol{y^q})$ defines a convex set of sampled signals such that all of them are quantized to the same quantization bins (see Fig. 3(a)).

The second set of constraints $\boldsymbol{S_2}$ comes from the fact that the signal $y(t)$, obtained after filtering $x(t)$, is periodic and bandlimited.

Set $\boldsymbol{S_2}$: Set of N-periodic discrete-time signals bandlimited to $2M+1$ non-zero DTFS components.

In addition to the fact that the N-periodic discrete-time signals should have $2M+1$ nonzero DTFS components we also want to make use of the structure of the signal $x(t)$, namely, that is a periodic stream of Diracs. Therefore, we define another set of constraints, as follows:

Set $\boldsymbol{S_3}$: Set of N-periodic discrete-time signals, such that the $\{Y[m]\}_{m=-M}^{M}$ DTFS components originate from a periodic stream of Diracs, that is $Y[m] = X[m] = \frac{1}{\tau}\sum_{k=0}^{K-1} c_k e^{-j2\pi m t_k/\tau}$, $m = -M, \ldots, M$, with $t_k, c_k \in \mathbb{R}$, $0 < t_k \leq \tau$, while there are no constraints on $Y[m]$ for $|m| > M$.

We can get more insight into the structure of the sets $\boldsymbol{S_1}, \boldsymbol{S_2}$ and $\boldsymbol{S_3}$ if we observe that $\boldsymbol{S_1}$ is an

[2]Another possibility to define the quantizer is to use the second type of quantizer, defined as $y_n^q = Q(y_n) = \Delta\lfloor y_n/\Delta \rfloor$. Any choice of the quantizer is not going to have any influence on our results

N-dimensional hypercube in the N-dimensional space $\mathcal{H}$, $\boldsymbol{S_2}$ is an $(2M+1)$-dimensional subspace of $\mathcal{H}$, and that $\boldsymbol{S_2} \cap \boldsymbol{S_3}$ is a $(2K)$-dimensional (nonlinear) surface inside $\boldsymbol{S_2}$. This dimensional argument naturally brings the notation of oversampling by space dimension ratios: $N/(2M+1)$ and $(2M+1)/(2K)$.

Now, we are going to define projections on the corresponding sets.

Projection $\boldsymbol{P_1}$: Given a set of samples $\boldsymbol{y}$, $\boldsymbol{y_1} = \boldsymbol{P_1}(\boldsymbol{y})$ is obtained as:

1) if $y_n \in \boldsymbol{S_1}$, then $y_{1,n} = y_n$.
2) else, $y_{1,n}$ is taken to be equal to the closest border of the quantization interval $Q^{-1}(y_n^q)$, that is, $\boldsymbol{P_1}(y_n) = y_n^q + \text{sign}(y_n - y_n^q)\frac{\Delta}{2}$.

Projection $\boldsymbol{P_2}$: Given an N-periodic discrete time signal $\boldsymbol{y}$, $\boldsymbol{y_2} = \boldsymbol{P_2}(\boldsymbol{y})$ is obtained by lowpass filtering, such that the nonzero DTFS components are $Y_2[m] = Y[m]$ for $m = -M, \ldots, M$.

Projection $\boldsymbol{P_3}$: Given an N-periodic discrete time signal $\boldsymbol{y}$, the projection $\boldsymbol{P_3}$ provides a new signal $\boldsymbol{y_3} = \boldsymbol{P_3}(\boldsymbol{y})$, with the set of in-band DTFS $\{Y_3[m]\}_{m=-M}^{M}$ that are $Y_3[m] = \frac{1}{\tau}\sum_{k=0}^{K-1} c_k e^{-j\frac{2\pi m t_k}{\tau}}$, $m = -M, \ldots, M$, with $t_k, c_k \in \mathbb{R}$, $0 < t_k \leq \tau$ while the out-band DTFS remain the same, i.e. $Y[m] = Y_3[m]$ for $|m| > M$.

Projection $\boldsymbol{P_3}$ involves augmenting the matrix in (3) using $2M+1$ Fourier components. Notice that, since there is quantization taking place, we do not have the exact Fourier coefficients, but only estimates $Y_2[m] = \hat{X}[m]$, and therefore (3) does not have an exact solution. Therefore, in order to get better estimates of the time positions, we use a generalized form of (3), with an augmented equation system using the $2M+1$ Fourier component estimates and increasing the order of the annihilating filter, as follows:

$$\begin{pmatrix} Y_2[0] & Y_2[-1] & \ldots & Y_2[-L] \\ Y_2[1] & Y_2[0] & \ldots & Y_2[-L+1] \\ \vdots & \vdots & \ddots & \vdots \\ Y_2[M] & Y_2[M-1] & \ldots & Y_2[M-L] \end{pmatrix} \begin{pmatrix} a_0 \\ a_1 \\ \vdots \\ a_L \end{pmatrix} \simeq \begin{pmatrix} 0 \\ 0 \\ \vdots \\ 0 \end{pmatrix} \tag{4}$$

where the left-hand-side matrix has a size $(M+1)\times(L+1)$ with $K \leq L \leq M$ and L is the filter order. In (4), we indicate with the symbol $\simeq$ that the system of equation is not exactly satisfied. Notice here how the oversampling in frequency is introduced by extending the number of rows from $K+1$ to $M+1$ and at the same time, making the order of the filter larger than K, that is $L \geq K$. By taking $a_0 = 1$, the

system (4) becomes equivalent to a high-order Yule-Walker (HOYW) system [12]:

$$\begin{pmatrix} Y_2[-1] & Y_2[-2] & \dots & Y_2[-L] \\ Y_2[0] & Y_2[-1] & \dots & Y_2[-(L-1)] \\ \vdots & \vdots & \ddots & \vdots \\ Y_2[M-1] & Y_2[M-2] & \dots & Y_2[M-L] \end{pmatrix} \begin{pmatrix} a_1 \\ a_2 \\ \vdots \\ a_L \end{pmatrix} \simeq - \begin{pmatrix} Y_2[0] \\ Y_2[1] \\ \vdots \\ Y_2[M] \end{pmatrix} \tag{5}$$

or in matrix notation,

$$\hat{\boldsymbol{H}}\boldsymbol{a} \simeq -\hat{\boldsymbol{h}} \tag{6}$$

where $\hat{\boldsymbol{h}} = [\ Y_2[0] \quad Y_2[1] \quad \dots Y_2[M]\ ]^T$, $\boldsymbol{a} = [\ a_1 \quad \dots \quad a_L\ ]^T$ and

$$\hat{\boldsymbol{H}} = \begin{pmatrix} Y_2[-1] & Y_2[-2] & \dots & Y_2[-L] \\ Y_2[0] & Y_2[-1] & \dots & Y_2[-(L-1)] \\ \vdots & \vdots & \ddots & \vdots \\ Y_2[M-1] & Y_2[M-2] & \dots & Y_2[M-L] \end{pmatrix}$$

Since both $\hat{\boldsymbol{H}}$ and $\hat{\boldsymbol{h}}$ are distorted from the original values, the use of Total Least Square (TLS) method, which allows for the fact that both $\hat{\boldsymbol{H}}$ and $\hat{\boldsymbol{h}}$ may have some error, instead of Least Square (LS) method is more appropriate [13]. Simulation results in [14] show that, in general, for solving HOYW equations the TLS method achieves the better accuracy than the LS method. This is particularly clear in cases where the zeros of the annihilating filter approach the unit circle [13]. As pointed out before, the order L of the annihilating filter may lie between K and M. So, there will be K "correct" or signal-related roots and $L-K$ extraneous roots, created artificially by the method. There are several ways to decide the positions of the "correct" roots. We propose two methods:

1) Choose the K roots that are closest to the unit circle. This is the common solution used for the retrieval of sinusoids in noise [15], which can be seen as a dual problem in the frequency domain.
2) Perform two steps:
   a) Compute roots without increasing the filter order.
   b) Compute roots increasing the filter order and choose the roots that are the closest to the roots in a).

Notice that by increasing M and L, extraneous roots can be very close to the unit circle and the first method might fail. Since the second method does not have this problem and we are primarily interested in the reconstruction accuracy for high oversamplings, we use the second method in this work.

If there was no quantization and the estimated $\{Y_2(m)\}_{m=-M}^{M}$ were the exact ones, then the chosen roots would all lie on the unit circle. However, because of the quantization error, an additional step is

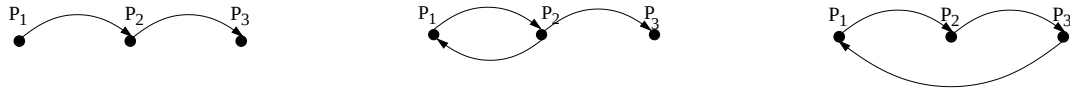

(a) (b) (c)

Fig. 4. (a) Non-consistent reconstruction algorithm consists of applying projections $\boldsymbol{P_1}$, $\boldsymbol{P_2}$ and $\boldsymbol{P_3}$ once; (b) The *Weak* consistency algorithm consists of first iterating projections $\boldsymbol{P_1}$ and $\boldsymbol{P_2}$, and then once applying projection $\boldsymbol{P_3}$; (c) The *Strong* consistency algorithm consists of iterating projections $\boldsymbol{P_1}$, $\boldsymbol{P_2}$ and $\boldsymbol{P_3}$.

required after the TLS projection, which consist of projecting the obtained roots to the unit circle, in order to get unit-norm root estimates $\hat{u}_k = e^{-j\frac{2\pi\hat{t}_k}{\tau}}$. From $\hat{u}_k$, we can directly compute the time positions $\{\hat{t}_k\}_{k=0}^{K}$. Then, using (1), we can estimate the weights $\{\hat{c}_k\}_{k=0}^{K}$. The whole process including the TLS projection, extracting the "correct" roots and computing the time positions and weights, can be seen as the third projection $\boldsymbol{P_3}$.

Notice that although we are primarily interested in the reconstruction $\hat{x}(t)$, we can consider reconstruction $\boldsymbol{y_3} \in \boldsymbol{S_2} \cap \boldsymbol{S_3}$ since there is one-to-one correspondence between the set of all possible inputs $x(t)$ and a subset of $\mathcal{H}$, which is exactly $\boldsymbol{S_2} \cap \boldsymbol{S_3}$. After defining the sets of constraints and the corresponding projections we are ready to formally define the non-consistent reconstruction and to introduce the two levels of consistency.

Definition 1: Reconstruction $\boldsymbol{y_3} = \boldsymbol{P_3}(\boldsymbol{P_2}(\boldsymbol{y^q}))$ is called a non-consistent reconstruction.

What makes this reconstruction non-consistent is the fact that after re-sampling and re-quantizing, the signal $\boldsymbol{P_2}(\boldsymbol{y^q})$ may not always lie in the same quantization bins as the original $\boldsymbol{y}$, or equivalently, it is possible that $\boldsymbol{P_2}(\boldsymbol{y^q}) \notin \boldsymbol{S_1} \cap \boldsymbol{S_2}$. Notice that, quantization applied to a signal that belongs to $\boldsymbol{S_1} \cap \boldsymbol{S_2}$ makes it leave $\boldsymbol{S_1} \cap \boldsymbol{S_2}$, although it still remains in the global space $\mathcal{H}$. Certain improvement can be achieved forcing some of the previously defined constraints. Therefore, we define *Weak* consistent reconstruction, as follows:

Definition 2: Reconstruction $\boldsymbol{y_3} \in \boldsymbol{P_3}(\boldsymbol{S_1} \cap \boldsymbol{S_2})$ is called *Weak* consistent reconstruction.

To impose the *Weak* consistent reconstruction, notice that sets $\boldsymbol{S_1}$ and $\boldsymbol{S_2}$ are convex sets and $\boldsymbol{P_1}$ and $\boldsymbol{P_2}$ are convex projections. Therefore, starting from the quantized samples $\boldsymbol{y^q}$ obtained from the original signal, and iterating only the projections $\boldsymbol{P_1}$ and $\boldsymbol{P_2}$, we will converge to $\boldsymbol{y_2} \in \boldsymbol{S_1} \cap \boldsymbol{S_2}$. The convergence is ensured by the theorem of alternating projections on convex sets (POCS) [15]. Moreover, in practice, numerically speaking, a *Weak* consistent reconstruction can be approached within a finite number of iterations. Once we have converged to the reconstruction $\boldsymbol{y_2} \in \boldsymbol{S_1} \cap \boldsymbol{S_2}$, we apply the additional projection $\boldsymbol{P_3}$, over the set $\boldsymbol{S_3}$ to obtain $\boldsymbol{y_3} \in \boldsymbol{P_3}(\boldsymbol{S_1} \cap \boldsymbol{S_2}) \subset \boldsymbol{S_2} \cap \boldsymbol{S_3}$. The *Weak* consistency algorithm is illustrated in Fig. 4(b).

Notice that, as opposed to the sets $\boldsymbol{S_1}$ and $\boldsymbol{S_2}$, which do not contain any information about the structure of the signal $x(t)$, the set $\boldsymbol{S_3}$ use the knowledge about the Fourier coefficients originated from a stream of Diracs. Following the idea of *Weak* consistent reconstruction we can extend the concept of consistency to not only the two sets $\boldsymbol{S_1}$ and $\boldsymbol{S_2}$ but also $\boldsymbol{S_3}$. These three sets are used to enforce a stronger sense of consistency, that is called *Strong* consistency and is defined as follows:

Definition 3: Reconstruction $\boldsymbol{y_3} \in \boldsymbol{S_1} \cap \boldsymbol{S_2} \cap \boldsymbol{S_3}$ is called *Strong* consistent reconstruction.

The concept of the *Strong* consistency adds a third property in addition to the previous two properties defined by the concept of *Weak* consistency. Similarly to the *Weak* consistency algorithm we can define a *Strong* consistency algorithm, where we generalize the idea of alternating projections to more than two projections. We form a composite projection by the sequential application of $\boldsymbol{P_1}$, $\boldsymbol{P_2}$ and $\boldsymbol{P_3}$ and the goal is to converge to a point in the intersection set $\boldsymbol{S_1} \cap \boldsymbol{S_2} \cap \boldsymbol{S_3}$. In practice, we have to check that the reconstructed signal $\boldsymbol{y_2}$ (see Fig. 1) is the result of filtering a periodic stream of Diracs. In terms of Fourier coefficients, *Strong* consistent reconstruction means that $\boldsymbol{y_2}$ has Fourier coefficients satisfying (1). Notice that although for high enough oversampling, the projection $\boldsymbol{P_3}$ is convex, the set $\boldsymbol{S_3}$ is not convex. In general, this could cause problems when iterating the composite projection $\boldsymbol{P_3 P_2 P_1}$, because while any projection $\boldsymbol{P_i}$ mapping to $\boldsymbol{S_i}$ will reduce (more precisely, not increase) the distance to $\boldsymbol{S_i}$, if one of the sets is not convex, we could still get an increase in distance to the intersection set $\boldsymbol{S_1} \cap \boldsymbol{S_2} \cap \boldsymbol{S_3}$. Here, we conjecture that for large enough R_t and R_f, the convergence property is ensured. Our experimental results in Section VI confirm clearly this conjecture. The *Strong* consistency algorithm is illustrated in Fig. 4(c). Notice that the complexity of the *Strong* consistent reconstruction is higher than the *Weak* consistent algorithm, because it involves iterations of all three projections.

To illustrate the fact that *Strong* consistency introduces one more set of constraints and hence reduces the set of possible reconstructions, as compared to *Weak* consistency, we remark that

$$\boldsymbol{S_1} \cap \boldsymbol{S_2} \cap \boldsymbol{S_3} \subset \boldsymbol{S_3} \quad \Rightarrow \quad \boldsymbol{P_3}(\boldsymbol{S_1} \cap \boldsymbol{S_2} \cap \boldsymbol{S_3}) = \boldsymbol{S_1} \cap \boldsymbol{S_2} \cap \boldsymbol{S_3}.$$

On the other hand,

$$\boldsymbol{P_3}(\boldsymbol{S_1} \cap \boldsymbol{S_2} \cap \boldsymbol{S_3}) \subset \boldsymbol{P_3}(\boldsymbol{S_1} \cap \boldsymbol{S_2}),$$

that confirms that the set of *Strong* consistent reconstruction is a subset of the *Weak* consistent reconstruction set. This implies that by enforcing *Strong* consistency in our reconstruction, on average, the reconstruction will be closer (or the same, but never further) to the original signal, than in the case of enforcing only *Weak* consistency.

It is important to note that, since $\boldsymbol{y_2}$ is a bandlimited signal, there exist algorithms [16], [17], [18] for reconstructing $\boldsymbol{y_2}$ which do not require iterated projections and which achieve a similar reconstruction accuracy as the one shown in Theorem 1 (see Section V). These algorithms could then be followed by projection $\boldsymbol{P_3}$ in order to achieve a performance similar to the *Weak* consistency algorithm. However, the algorithms in [16], [17], [18] do not ensure the consistency with respect to the quantization bins, which means that they can not be used, together with projection $\boldsymbol{P_3}$, in order to achieve *Strong* consistency. More specifically, iterating the algorithms in [16], [17], [18] together with projection $\boldsymbol{P_3}$, we will be like projecting only on the space $\boldsymbol{S_2}$ and $\boldsymbol{S_3}$. In our *Strong* consistent reconstruction algorithms (see Fig. 4(c)), by projecting on the additional set $\boldsymbol{S_1}$, we reduce the set of possible reconstructions, and consequently, we increase further the reconstruction accuracy.

A. Extension to other non-bandlimited signals with finite rate of innovations

Our reconstruction algorithms can be applied to other types of signals with finite rate of innovation, such as finite (non-periodic) streams of Diracs and periodic nonuniform splines, where oversampling in time and in frequency can be again introduced.

The reconstruction of finite streams of Diracs from filtered unquantized samples, is explained in [1]. Basically, after getting the filtered samples y_n, using a sinc sampling kernel, an annihilating discrete-time filter method is used to obtain first the time positions and then the weights. In the case of quantization, after quantizing the samples y_n, as before, we can project to the space of (non-periodic) bandlimited signals, with bandwidth determined by the oversampling in frequency, and check if the new samples $\hat{y}_n$ belongs to the corresponding quantization bins. If this is not the case, we can perform projection $\boldsymbol{P_1}$, as before. Similarly to $\boldsymbol{P_3}$, we can define a projection on the signal space of finite streams of Diracs.

Analyzing periodic non-uniform splines, we can see that the $(S+1)$th derivative of a periodic nonuniform spline of degree S with knots at $\{t_k\}_{k=0}^{K-1}$ is given by a periodic stream of K Diracs. This allows us to extend easily the reconstruction algorithm to the case of nonuniform splines. The $(S+1)$th derivative of a nonuniform spline $x^{(S+1)}(t)$ has Fourier coefficients given by:

$$X^{(S+1)}[m] = \frac{1}{\tau}\sum_{k=0}^{K-1} c_k e^{-j2\pi m t_k}$$

Differentiating (1) $S+1$ times we see that, the Fourier coefficients $X^{(S+1)}[m]$ are related to the Fourier coefficients $X[m]$ of the corresponding stream of Diracs that has time positions $\{t_k\}_{k=0}^{K-1}$ and weights $\{c_k\}_{k=0}^{K-1}$, in the following way:

$$X^{(S+1)}[m] = (j2\pi m/\tau)^{(S+1)} X[m], \quad m \in \mathcal{Z}.$$

Therefore, we can use the same consistent reconstruction algorithms for reconstructing the time positions and weights of Diracs, providing the final reconstruction of the nonuniform splines.

V. Theoretical Performance of Oversampling

A. Error in Time Positions $\{t_k\}$

As explained in the previous section, in order to estimate the time positions and weights, some of the consistency constraints that we enforce involve the N-periodic band-limited $(M \leq N)$ discrete-time signal $\boldsymbol{y_2}$. We can easily change the bandwidth of the signal $\boldsymbol{y_2}$, by increasing/decreasing the bandwidth of the sampling kernel h_B, which is equivalent to changing the oversampling ratio in frequency R_f. Notice that by changing the bandwidth, we change the signal $\boldsymbol{y_2}$. In terms of DTFS, increasing/decreasing the bandwidth is equivalent to adding/removing nonzero DTFS. Similarly, for the fixed bandwidth of the sampling kernel we still can choose how many samples $\boldsymbol{y}$ we want to have, that is, what will be the oversampling ratio in time R_t. In the following we are going to see what is the dependence of the reconstruction quality on R_t and R_f. As a quantitative characterization of the reconstruction quality we introduce the following distances:

1) $d_1(\boldsymbol{y}, \boldsymbol{y'}) = MSE(\boldsymbol{y}, \boldsymbol{y'}) = MSE(\boldsymbol{Y}, \boldsymbol{Y'})$ where the last equality comes from the Parseval theorem;
2) $d_2(\boldsymbol{y}, \boldsymbol{y'}) = MSE(\boldsymbol{P_3}(\boldsymbol{P_2}(\boldsymbol{y})), \boldsymbol{P_3}(\boldsymbol{P_2}(\boldsymbol{y'})))$;
3) $d_3(\boldsymbol{y}, \boldsymbol{y'}) = MSE(\boldsymbol{t}, \boldsymbol{t'})$ for $\boldsymbol{y} \in \boldsymbol{S_2} \cap \boldsymbol{S_3}$;
4) $d_4(\boldsymbol{y}, \boldsymbol{y'}) = MSE(\boldsymbol{c}, \boldsymbol{c'})$ for $\boldsymbol{y} \in \boldsymbol{S_2} \cap \boldsymbol{S_3}$.

In practice, the distances d_2, d_3 and d_4 are the most interesting. However, in some of our proofs and developments involving d_3, we need to make use of the distance d_1 for the case of $\boldsymbol{y} \in \boldsymbol{S_1} \cap \boldsymbol{S_2}$ as an intermediate step. Later we show theoretically that d_4 depends on d_3 and we also show experimentally that d_1 does not differ too much from d_2 when $\boldsymbol{y} \in \boldsymbol{S_1} \cap \boldsymbol{S_2}$ (see Fig. 5). For the *Strong* consistent reconstruction the distances d_2 and d_3, where $\boldsymbol{y} \in \boldsymbol{S_1} \cap \boldsymbol{S_2} \cap \boldsymbol{S_3}$, are experimentally shown in the next section.

Theorem 1: Given the two N-periodic discrete time signals $\boldsymbol{y}, \boldsymbol{y'} \in \boldsymbol{S_1} \cap \boldsymbol{S_2}$ where the sets $\boldsymbol{S_1}$ and $\boldsymbol{S_2}$ are uniquely determined by $x(t)$, R_t and R_f, there exists an N_0 such that if $N \geq N_0$, there is a constant $c > 0$, which depends only on $x(t)$ and not on R_t and R_f, such that:

$$d_1(\boldsymbol{y}, \boldsymbol{y'}) \leq \frac{c}{R_t^2}.$$

Proof: see Appendix I.

The importance of this theorem is that even if we increase R_f, while keeping the R_t constant, the upper bound of d_1 remains the same. However, it is clear that since, we estimate the time positions from DTFS of $\boldsymbol{y_2}$, the number of available Fourier components in addition to d_1 directly impacts d_3. That is, increasing R_f, intuitively will improve the time positions estimates. On the other hand, notice also that, since from Theorem 1 d_1 will decrease as we increase R_t, then d_3 will decrease as we increase both R_t and R_f. Here, we also remark that increasing R_t or/and R_f, we also increase the number of samples since $N = (2K+1)R_tR_f$.

In the following theorem, we examine the order of dependence of d_3 as a function of both oversamplings R_t and R_f, for the case of *Weak* consistent reconstruction.

Theorem 2: Given the two N-periodic discrete time signals $\boldsymbol{y}, \boldsymbol{y'} \in \boldsymbol{S_1} \cap \boldsymbol{S_2}$ where the sets $\boldsymbol{S_1}$ and $\boldsymbol{S_2}$ are uniquely determined by $x(t)$, R_t and R_f, there exist some constants $a \geq 1$ and $b \geq 1$, such that if $R_t \geq a$ and $R_f \geq b$, there is a constant $c' > 0$ which depends only on $x(t)$ and not on R_t and R_f, and it holds that:

$$d_3(\boldsymbol{y}, \boldsymbol{y'}) \leq \frac{c'}{R_f^3 R_t^2}.$$

Proof: see Appendix II.

From Theorem 2 it can be seen that if we are limited to the some large but finite number of samples and $N \gg 2K+1$, by increasing R_f we reduce the d_3 faster than by increasing R_t. Thus, if we are allowed to use a fixed number of samples N and our goal is to minimize only d_3 we will tend to increase oversampling in frequency, R_f. In Sections VII and VIII the influence of increasing the R_t and R_f on the required bit-rate and error-rate dependence will be considered as well.

B. Error in Weights $\{c_k\}$

Given the time position estimates $\{\hat{t}_k\}$ we can directly estimate the weights $\{\hat{c}_k\}$ from (1) as:

$$\begin{pmatrix} X[0] \\ X[1] \\ \vdots \\ X[M] \end{pmatrix} = \frac{1}{\tau} \begin{pmatrix} 1 & 1 & \cdots & 1 \\ u_0 & u_1 & \cdots & u_{K-1} \\ \vdots & \vdots & \cdots & \vdots \\ u_0^M & u_1^M & \cdots & u_{K-1}^M \end{pmatrix} \begin{pmatrix} c_0 \\ c_1 \\ \vdots \\ c_{K-1} \end{pmatrix} \tag{7}$$

Notice here, that the Fourier coefficients are the one that comes as the result of the projection $\boldsymbol{P_2}$, that is $\boldsymbol{X} = \boldsymbol{Y_2}$. We can also write the previous equation in the matrix notation as follows:

$$\boldsymbol{Y_2} = \frac{1}{\tau} \boldsymbol{V} \boldsymbol{C}.$$

Notice that the matrix $\boldsymbol{V}$ has $M \geq K$ rows, due to the oversampling in time, which implies that the system in (7) is overdetermined. Thus, we can compute $\boldsymbol{C}$ in the two ways, using a TLS projection or a LS projection. In the latter case, $\boldsymbol{C}$ given by:

$$\boldsymbol{C} = (\boldsymbol{V}^H \boldsymbol{V})^{-1} \boldsymbol{V}^H \boldsymbol{Y_2}$$

The error in vector $\boldsymbol{C}$ defined by d_4 depends directly on the error in $\boldsymbol{Y_2}$, which is equal to d_1 in the case of *Weak* consistent reconstruction and on the error in $\boldsymbol{V}$ which is related to the error in time positions, i.e. d_3. Hence,

$$d_4(\boldsymbol{y}, \boldsymbol{y'}) = f(d_1(\boldsymbol{y}, \boldsymbol{y'}), d_3(\boldsymbol{y}, \boldsymbol{y'})) \quad \text{for} \quad \boldsymbol{y}, \boldsymbol{y'} \in \boldsymbol{S_1} \cap \boldsymbol{S_2}.$$

Because of this dependence, in this work, we focus on the error related to DTFS and the error in time positions. Moreover, in many practical applications, such as UWB communications (e.g. PPM modulation) and sensor networks sampling local physical sources, the important information is given by time positions.

VI. Experimental Performance of Oversampling

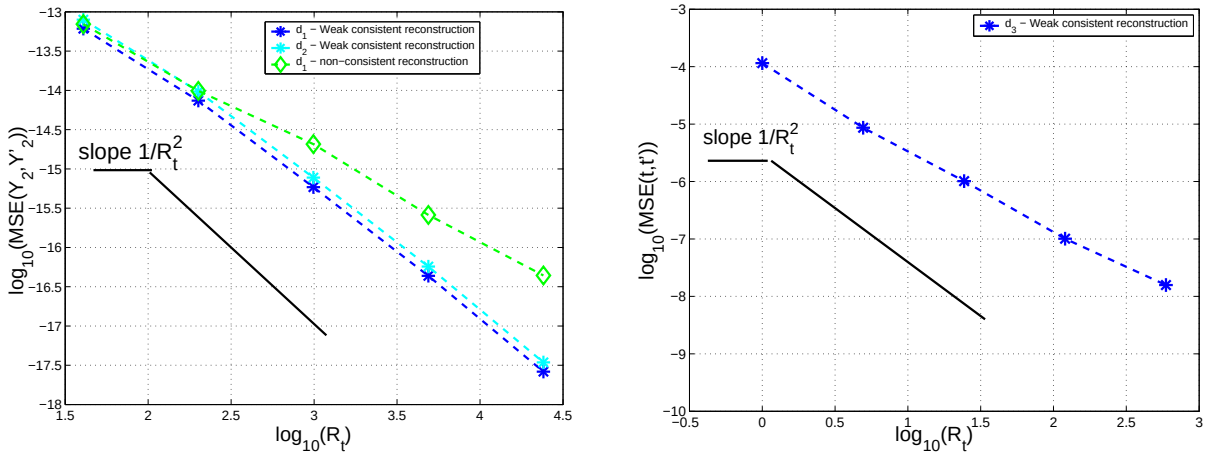

(a) (b)

Fig. 5. The *Weak consistent reconstruction. Dependence of accuracy on oversampling in time* R_t *for: (a)* d_1 *- MSE of Fourier coefficients where* $X[m] = Y_2[m]$ *and* $Y_2'[m]$ *is the reconstruction where* $\boldsymbol{y_2} \in \boldsymbol{S_1} \cap \boldsymbol{S_2}$*; (b)* d_3 *- MSE of time positions.*

In this section, we show experimental results for the three algorithms illustrated in Fig. 4, with parameters: $K = 2$, $\tau = 10$, $t_k \in (0, \tau]$, $c_k \in [-1, 1]$. The positions and the weights are randomly chosen from the corresponding intervals and the results are the average over 300 signals. For the *Weak* consistency algorithm, our numerical results confirm Theorems 1 and Theorem 2, with a performance of

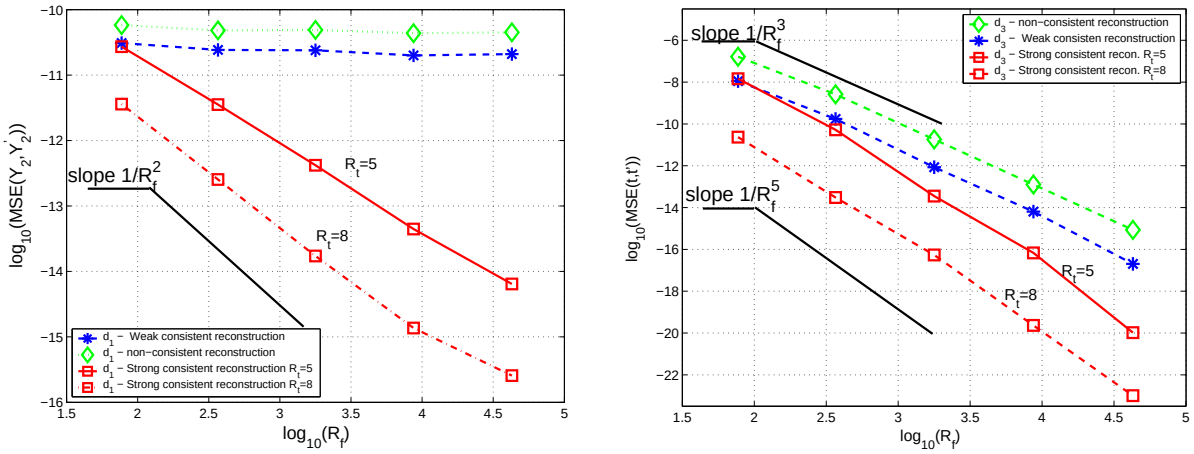

(a) (b)

Fig. 6. The *Non-consistent, Weak consistent and Strong consistent reconstruction. Dependence of accuracy on oversampling in frequency R_f for: (a) MSE of Fourier coefficients $X[m] = Y_2[m]$; (b) MSE of time positions.*

$O(1/R_t^2 R_f^3)$, illustrated in Fig. 5 and Fig. 6. The *Strong* consistency algorithm provides an experimental behaviour of $O(1/R_t^2 R_f^5)$ that is also illustrated in Fig. 6. We have compared our consistent reconstruction algorithms with the case of non-consistent reconstruction. A clear outperformance of our reconstruction algorithms over non-consistent reconstructions is observed (see Fig. 5(a), 6).

We can conclude that by increasing the oversampling in frequency R_f, we can achieve a reconstruction accuracy which is (polynomially) superior for both the *Weak* and the *Strong* consistency algorithms than the one obtained by increasing R_t. Moreover, from the results of MSE dependence on the quantization stepsize derived in Section VIII, we also conclude that oversampling in frequency outperform decreasing of the quantization stepsize Δ. Therefore, oversampling in frequency provides largest gain in performance.

Next, we analyze encoding schemes and the scaling laws that can be achieved in terms of bit rate and error-rate dependence.

VII. Encoding Scheme and Bit Rate

As explained in Section III, by increasing R_t or R_f, we increase the number of samples $\{y_n\}$. It is clear that using the traditional way of encoding, that is, pulse-code modulation (PCM) encoding, the bit rate depends linearly on the number of samples N and for each sample, using a scalar quantizer with stepsize Δ, we need at most $1 + \log_2(d_y/\Delta)$ bits, where d_y denotes the dynamic range in amplitude of the signal $y(t)$. From (15) it can be easily shown that

$$d_y \leq 2\left(\sum_{k=0}^{K}|c_k|\right)\frac{2M+1}{\tau} \Longrightarrow d_y = O(R_f), \tag{8}$$

and we assume that the weights are bounded by some fixed bounds, that is, $c_k \in [-a, a]$. Hence, for a fixed Δ, the bit rate can be bounded as:

$$B_{PCM} = \frac{N}{\tau}\left(1+\log_2\left(\frac{d_y}{\Delta}\right)\right) = N\ O(\log_2(R_f)) = O(R_t R_f \log_2 R_f). \tag{9}$$

On the other hand, when the sampling interval is sufficiently fine, some simple and efficient techniques can be developed [10], for which the required bit rate is substantially smaller than in the case of PCM encoding. In the following, we show how to make use of the results in [10], developed for bandlimited signals to compute the dependence of the bit rate on both R_t and R_f, for our problem.

The idea originates from the equivalence between the traditional interpretation of the digital version of an analog signal, where the uncertainty is determined by the quantization stepsize at the exact time instants, and the alternative one [10], [19], where the digital signal is uniquely determined by the sampling intervals in which its quantization threshold crossings occur. A unique representation in the alternative interpretation is ensured if the following two conditions are satisfied: 1) the quantization threshold crossings are sufficiently separated, 2) at most one quantization threshold crossing occurs in each sampling interval. The first condition requires that the intervals between consecutive crossings through any given threshold are limited from below by a constant $T_1 > 0$. The second condition is satisfied if the slope of the signal is finite, which is ensured by the fact that the signal $y(t)$ has finite energy and is bandlimited. Thus, there is always an interval $T_2 > 0$ on which $y(t)$ cannot go through more that one quantization threshold crossing. For a sufficiently fine sampling period, that is $T_s \leq \min(T_1, T_2)$, all quantization threshold crossings occur in distinct sampling intervals, and a unique representation is ensured.

The encoded information, in the case of threshold crossings (TC) based encoding, are the positions of the sampling time intervals in which the quantization threshold crossings occur. The signal is observed in a given time interval, which in our case is the period τ. For determining the position of each sampling interval of length $T_s = \tau/N$, we need at most $1 + \log_2(\tau/T_s)$ bits. Every threshold crossing can be determined with respect to the previous one by introducing only one additional bit to indicate the direction, upwards or downwards, of the next threshold crossing. If C quantization threshold crossings occur during the period τ, then the required bit rate is $B_{TC} = C(2 + \log_2(T_s/\tau))$.

Next, we need to determine the maximal number of threshold crossings. There are two types of threshold crossings: 1) a d-crossing which is preceded by a threshold crossing of a different threshold level (Fig. 3(a) - first and second treshold crossing), and 2) an s-crossing which is preceded by a crossing of the same

threshold level (Fig. 3(a) - second and third treshold crossing). The sum of these two types of threshold crossings is the total number of threshold crossings per period τ. From results on non-harmonic Fourier expansions [20], the s-crossings for the case of bandlimited signals constitute a sequence of uniform density[3] ρ, which equivalently means that the zeros of the first derivative of $y(t)$ constitute a sequence of the same density. Then, ρ is bounded as $\rho = O(f_{max}) = O(R_f)$, where f_{max} is the maximum frequency of the signal $y(t)$ and it is of the order of the bandwidth B. Consequently, the number of s-crossings C_s is given by $C_s = O(f_{max}) = O(R_f)$. The maximum possible number of d-crossings C_d depends linearly on the maximum dynamic range d_y of the signal $y(t)$, that is $C_d = O(\frac{d_y}{\Delta}) = O(R_f)$ and., as it is shown in (8), depends linearly on R_f, hence, the same dependence holds for the number of d-crossings, that is, $C_d = O(R_f)$. Therefore,

$$B_{TC} \leq c_3 R_f (2 + \log_2(c_4 R_t R_f)), \tag{10}$$

where c_3 and c_4 are some constants that depend on the specific signal $x(t)$ and on the quantization stepsize Δ, but which do not depend on R_t and R_f. The additional bits required for specifying the first threshold crossing (the others are going to be specified with respect to this one) have arbitrary small effect on the required bit rate over the sufficiently long time period.

Comparing (9) and (10), we can conclude that the TC based encoding has clear advantages over the traditional PCM encoding, since the bit-rate for TC based encoding grows much more slowly as a function of the oversampling in time R_t. We also remark that these coding results are applicable regardless of the reconstruction method that is used (e.g. consistent or non-consistent reconstruction).

VIII. Error-Rate Dependence

A natural question that arises in oversampled A/D conversion is to compare the improvement in error-rate that comes, on the one hand, from the oversamplings, in our case from increasing R_t and R_f, and on the other hand, from reducing the quantization stepsize Δ. For the measure of the error-rate dependence, we consider the MSE of the time positions, as a function of the bit rate.

We have shown in Section V what is the dependence of both the MSE of time positions and the bit rate as a function of the oversampling ratios R_t and R_f. In this section, we also introduce the dependence

[3]A sequence λ_n of real or complex numbers has uniform density ρ, $\rho \geq 0$, if there are constants $L \leq \infty$ and $s > 0$ such that: a) $|\lambda_n - \frac{n}{\rho}| \leq L, n \in \mathbb{Z}$, b) $|\lambda_n - \lambda_m| \geq s > 0, \quad \text{where} n \neq m.$

of the MSE of time positions and the bit rate on the quantization stepsize Δ, and then we examine the error-rate dependence considering all the three parameters, R_t, R_f and Δ.

It has been shown in [10] that if: 1) there is a large number of quantization levels compared to the signal amplitude range, and 2) the quantization stepsize Δ is sufficiently small, then, it is approximately correct to model the quantization error as a uniformly distributed white noise over the interval $[-\Delta/2, \Delta/2]$ that is independent of the input signal. Assuming the white noise based model, we have:

$$MSE(y(t), \hat{y}(t)) = MSE(\boldsymbol{Y_2}, \hat{\boldsymbol{Y}}_{\boldsymbol{2}}) = \Delta^2/12.$$

Recall from Section II that we estimate the time positions from the Fourier coefficients $X[m] = Y_2[m]$, hence, the error for the time positions can be computed to a first order approximation[4] as:

$$\begin{aligned} \mathcal{E}(t_k) &= \sum_{m=-M}^{M} \frac{\partial t_k}{\partial Y_2[m]}\, \mathcal{E}(Y_2[m]) \\ |\mathcal{E}(t_k)|^2 &\leq \left(\sum_{m=-M}^{M} \left| \frac{\partial t_k}{\partial Y_2[m]} \right|^2 \right) \left(\sum_{m=-M}^{M} |\mathcal{E}(Y_2[m])|^2 \right) = \xi\, MSE(\boldsymbol{Y_2}, \hat{\boldsymbol{Y}}_{\boldsymbol{2}}) \end{aligned} \tag{11}$$

where $\xi = \sum_{m=-M}^{M} \left| \frac{\partial t_k}{\partial Y_2[m]} \right|^2$ measures the dependence of the time positions on the Fourier coefficients and does not depend on the quantization stepsize Δ. The inequality in (11) follows simply from Cauchy-Schwartz inequality. Therefore, for sufficiently small Δ it holds that:

$$MSE(\boldsymbol{t}, \hat{\boldsymbol{t}}) = O(\Delta^2). \tag{12}$$

Concerning the bit rate, it is clear that increasing/decreasing the quantization stepsize, we reduce/increase the required bit rate.

In the case of PCM encoding, for a fixed R_t and R_f, it can be seen from (9) that, the bit rate, as a function of the quantization stepsize Δ, is given by:

$$B_{PCM} = N \left(1 + \log_2 \left(\frac{d_y}{\Delta} \right) \right) = O \left(\log_2 \left(\frac{1}{\Delta} \right) \right). \tag{13}$$

In the case of TC based encoding, the dependence of the bit-rate on the quantization step size Δ comes through the dependence on the maximum number of threshold crossings, namely, $C_{max}(\Delta) = O(1/\Delta)$, which together with (10) and taking into account that now R_t and R_f are kept constant, results in:

$$B_{TC} \leq c_5 \frac{1}{\Delta} R_f (2 + \log_2(c_4 R_t R_f)) = O \left(\frac{1}{\Delta} \right), \tag{14}$$

[4]We assume sufficiently high enough oversamplings and sufficiently small quantization stepsize, so that the first order approximation is correct.

TABLE I

ERROR-RATE DEPENDENCE

Encoding method	Variation	Bit rate	*Weak* consistency - theory		*Strong* consistency - experiments	
			$MSE(\boldsymbol{t},\hat{\boldsymbol{t}})$	error-rate	$MSE(\boldsymbol{t},\hat{\boldsymbol{t}})$	error-rate
Threshold crossing encoding	R_t	$O(\log_2 R_t)$	$O(1/R_t^2)$	$O(2^{-2\alpha B_{TC}})$	$O(1/R_t^2)$	$O(2^{-2\alpha B_{TC}})$
	R_f	$O(R_f \log_2 R_f)$	$O(1/R_f^3)$	$O(B_{TC}^{-3})$	$O(1/R_f^5)$	$O(B_{TC}^{-5})$
	Δ	$O(1/\Delta)$	$O(\Delta^2)$	$O(B_{TC}^{-2})$	$O(\Delta^2)$	$O(B_{TC}^{-2})$
PCM encoding	R_t	$O(R_t)$	$O(1/R_t^2)$	$O(B_{PCM}^{-2})$	$O(1/R_t^2)$	$O(B_{PCM}^{-2})$
	R_f	$O(R_f \log_2 R_f)$	$O(1/R_f^3)$	$O(B_{PCM}^{-3})$	$O(1/R_f^5)$	$O(B_{PCM}^{-5})$
	Δ	$O(\log_2(1/\Delta))$	$O(\Delta^2)$	$O(2^{-2\beta B_{PCM}})$	$O(\Delta^2)$	$O(2^{-2\beta B_{PCM}})$

where B_{TC} denotes the bit rate corresponding to TC based encoding and c_5 is some constant that does not depend on R_t, R_f and Δ. All the results, for the $MSE(\boldsymbol{t},\hat{\boldsymbol{t}})$ and the bit rate, are given in Table I.

Analyzing Table I, we can see first that in the case of PCM encoding, the best error-rate dependence is obtained by decreasing the quantization stepsize Δ instead of increasing any type of oversampling. Since we have a logarithmic increase $O(\log_2(1/\Delta))$ of the bit rate and an error decrease of $O(\Delta^2)$, changing the stepsize Δ and fixing the oversampling ratios, we get a dependence of MSE of the order of $O(2^{-2\beta B_{PCM}})$, where β is some constant that does not depend on B_{PCM}. Assuming PCM encoding, this performance can not be achieved by increasing the oversampling ratios R_t and R_f. However, using the TC based encoding, we can achieve the same dependence (as when reducing the quantization stepsize Δ), by increasing the oversampling in time R_t. This is very important because, in practice, the cost (complexity of expensive high-precision analog circuitry) of halving Δ is much higher than that of doubling R_t. However, by increasing the oversampling in frequency R_f, the required bit rate grows exponentially faster than in the case of increasing R_t or decreasing Δ. Therefore, asymptotically (high rates), the error-rate performance obtained by increasing R_f is inferior to that of increasing R_t or decreasing Δ.

IX. CONCLUSIONS AND FUTURE WORK

In this paper, we studied reconstruction of non-bandlimited signals with finite rate of innovation, particularly, periodic streams of Diracs, under the presence of quantization. High reconstruction accuracy is obtained by introducing the oversampling in time and in frequency, and enforcing the concept of consistency. We defined the concept of *Weak* and *Strong* consistency and we examined the performance in terms of MSE of time positions, that is achieved with *Weak* and *Strong* consistent reconstruction algorithms. We concluded that the oversampling in frequency provides a superior decrease in MSE of

time positions. On the other hand, in terms of error-rate dependence, by using a threshold crossing based encoding, the oversampling in time provides a superior error-rate trade-off over the oversampling in frequency. Moreover, it is also observed that the error-rate dependence obtained from doubling the oversampling in time is the same as the one obtained from halving the quantization stepsize, while, in practice, the cost of performing the oversampling in time is much lower than that of reducing the quantization stepsize.

Some future lines of research include finding faster consistent reconstruction algorithms, such as algorithms which do not require projection iterations, extension of our results of A/D conversion for the case of more general sampling kernels (e.g. Gaussian kernels), reconstruction of signals with finite rate of innovations under physics based kernels, such as those given by a heat diffusion equation [5], and extension of our results to multidimensional non-bandlimited signals with finite rate of innovations.

APPENDIX I
PROOF OF THEOREM 1

In order to prove Theorem 1, we need first to compute the slope of the filtered signal $y(t)$. This signal is nothing but the sum of "$2M+1$-periodized" sinc functions, that is:

$$y(t) = \sum_{k=0}^{K} c_k \frac{\sin((2M+1)(t-t_k)\pi/\tau)}{\sin((t-t_k)\pi/\tau)} \tag{15}$$

It is then obvious that the slope of $y(t)$ is of the following order:

$$\frac{dy(t)}{dt} = \begin{cases} O(1), & \text{for} \quad t = t_k \\ O(R_f) & \text{otherwise.} \end{cases} \tag{16}$$

Using the results on oversampled A/D conversion of band-limited signals in $L^2(\mathbb{R})$ [10], it can be shown that in the case of stable sampling[5] [21], which is satisfied by the class of periodic bandlimited signals, the $MSE(y(t), \hat{y}(t))$ can be written as follows:

$$MSE(y(t), \hat{y}(t)) \leq \frac{9}{4}\frac{B}{A}\frac{\tau^2}{N^2}||y'(t)||^2, \tag{17}$$

[5]Definition of stable sampling: A sequence of real numbers $(\lambda_n)_{n\in\mathcal{Z}}$ is said to be a sequence of stable sampling in the space of square-integrable π-bandlimited function, denoted by $\mathcal{V}_\pi$, if there exist two constants, $A > 0$ and $B < \infty$, such that for any f in $\mathcal{V}_\pi$, the following sequence holds:

$$A\int_{-\infty}^{\infty} |f(x)|^2 dx \leq \sum_n |f(\lambda_n|^2 \leq B\int_{-\infty}^{\infty} |f(x)|^2 dx$$

where A and B are some constants such that $A > 0$ and $B < \infty$ and they do not depend on the signal $y(t)$ (particularly, they come from the definition of stable sampling) and $||\cdot||$ is the $L^2(\mathbb{R})$ norm. Inserting (16) in (17) we get the final conclusion, that is:

$$d_1(\boldsymbol{y}, \hat{\boldsymbol{y}}) = MSE(y(t), \hat{y}(t)) \leq \frac{9}{4}\frac{B}{A}\frac{\tau^2}{(2K+1)^2 R_t^2 R_f^2} O(R_f^2) = O\left(\frac{1}{R_t^2}\right). \tag{18}$$

Here, $\boldsymbol{y}$ and $\hat{\boldsymbol{y}}$ are any two signals in $\boldsymbol{S_1} \cap \boldsymbol{S_2}$.

APPENDIX II
PROOF OF THEOREM 2

The annihilating filter method with oversampling in time and in frequency is the classical high-order Yule-Walker system (HOYW)[12]. In order to prove Theorem 2, we go through the two main steps:

1) We first show how the estimation accuracy is effected by:
   a) the number of YW equations, or equivalently, the oversampling in frequency R_f;
   b) the model order, or equivalently, the filter order L.

   For this purpose, we use a common singular value decomposition (SVD)-based HOYW procedure.
2) Then, we use the known result that the TLS-based HOYW method and the SVD-based HOYW method are asymptotically equivalent.

SVD-based method finds the rank-K (K being the number of Diracs) best approximation $\hat{\boldsymbol{H}}_K$ in the Frobenious norm sense and obtains the following solution:

$$\begin{aligned} \hat{\boldsymbol{H}}_K \hat{\boldsymbol{a}} &= -\hat{\boldsymbol{h}} \\ \hat{\boldsymbol{a}} &= -(\hat{\boldsymbol{H}}_K)^{\dagger} \hat{\boldsymbol{h}} \end{aligned}$$

where $(\cdot)^{\dagger}$ denotes the Moore-Penrose pseudoinverse of $(\cdot)$. In general, the matrix $\hat{\boldsymbol{H}}$ has full rank being equal to $\min(L, M)$ and $(\hat{\boldsymbol{H}})^{\dagger}$ does not approach $(\boldsymbol{H})^{\dagger}$ which has rank K, even for the case when M increases without bound. In contrast to $(\hat{\boldsymbol{H}})^{\dagger}$, the pseudoinverse $(\hat{\boldsymbol{H}}_K)^{\dagger} \rightarrow (\boldsymbol{H})^{\dagger}$ as the error in $\hat{X}[m]$ becomes smaller. This is a crucial property that is necessary for reducing the error in the estimates.

Suppose that $\boldsymbol{a}$ are the exact coefficients of the annihilating filter polynomial. Then, the following analysis holds:

$$\begin{aligned} \hat{\boldsymbol{a}} - \boldsymbol{a} &= -(\hat{\boldsymbol{H}}_K)^{\dagger} \hat{\boldsymbol{h}} - \boldsymbol{a} \\ &= -(\hat{\boldsymbol{H}}_K)^{\dagger} (\hat{\boldsymbol{h}} + \hat{\boldsymbol{H}}\boldsymbol{a} - \hat{\boldsymbol{H}}\boldsymbol{a}) - \boldsymbol{a} \\ &= -(\hat{\boldsymbol{H}}_K)^{\dagger} (\hat{\boldsymbol{h}} + \hat{\boldsymbol{H}}\boldsymbol{a}) + [(\hat{\boldsymbol{H}}_K)^{\dagger} \hat{\boldsymbol{H}} - \boldsymbol{I}]\boldsymbol{a} \\ &= -(\hat{\boldsymbol{H}}_K)^{\dagger} \boldsymbol{\xi} + [(\hat{\boldsymbol{H}}_K)^{\dagger} \hat{\boldsymbol{H}} - \boldsymbol{I}]\boldsymbol{a} \end{aligned} \tag{19}$$

where

$$\boldsymbol{\xi} = \hat{\boldsymbol{h}} + \hat{\boldsymbol{H}}\boldsymbol{a} = \left[\begin{array}{cc} \hat{\boldsymbol{h}} & \hat{\boldsymbol{H}} \end{array}\right] \left[\begin{array}{c} 1 \\ \boldsymbol{a} \end{array}\right].$$

First, we show what is the relationship between the matrix $\boldsymbol{\mathcal{P}_a} = (\hat{\boldsymbol{a}} - \boldsymbol{a})(\hat{\boldsymbol{a}} - \boldsymbol{a})^T$, associated to the annihilating filter coefficients and the matrix $\boldsymbol{\mathcal{P}_t} = (\hat{\boldsymbol{t}} - \boldsymbol{t})(\hat{\boldsymbol{t}} - \boldsymbol{t})^T$, associated to the time positions.

The angular positions of the roots of the annihilating filter give us the estimates of the time positions. Assuming that the roots are sufficiently close to the unit circle, so that the first approximation of the Taylor series expansion corresponding to the time positions holds, it can be shown [12] that:

$$\hat{t}_k - t_k = \frac{1}{2\pi} Re\left\{ \frac{\beta_k - j\alpha_k}{\alpha_k^2 + \beta_k^2} \boldsymbol{u_k}^T (\hat{\boldsymbol{a}} - \boldsymbol{a}) \right\}$$

with $\boldsymbol{u_k} = [u_k^{-1} u_k^{-2} \dots u_k^{-L}]^T$ or, in matrix form,

$$\hat{\boldsymbol{t}} - \boldsymbol{t} \;\; = \;\; \frac{1}{2\pi} Re\{\boldsymbol{F}\boldsymbol{G}(\hat{\boldsymbol{a}} - \boldsymbol{a})\}. \tag{20}$$

Therefore:

$$\boldsymbol{\mathcal{P}_t} \;\; = \;\; (\hat{\boldsymbol{t}} - \boldsymbol{t})(\hat{\boldsymbol{t}} - \boldsymbol{t})^T = \frac{1}{4\pi^2} Re\{\boldsymbol{F}\boldsymbol{G}(\hat{\boldsymbol{a}} - \boldsymbol{a})\} Re\{(\hat{\boldsymbol{a}} - \boldsymbol{a})^T \boldsymbol{G}^T \boldsymbol{F}^T\},$$

where:

$$\begin{aligned} \alpha_k &= \left[\begin{array}{cccc} \cos(2\pi t_k) & 2\cos(4\pi t_k) & \dots & L\cos(2L\pi t_k) \end{array}\right] \boldsymbol{a}, \\ \beta_k &= \left[\begin{array}{cccc} \sin(2\pi t_k) & 2\sin(4\pi t_k) & \dots & L\sin(2L\pi t_k) \end{array}\right] \boldsymbol{a}, \end{aligned}$$

$$\boldsymbol{F} = \left(\begin{array}{ccc} \frac{\beta_1 - j\alpha_1}{\alpha_1^2 + \beta_1^2} & & 0 \\ & \ddots & \\ 0 & & \frac{\beta_K - j\alpha_K}{\alpha_K^2 + \beta_K^2} \end{array}\right), \qquad \boldsymbol{G} = \left(\begin{array}{ccc} u_0^{-1} & \dots & u_0^{-L} \\ \vdots & & \vdots \\ u_{K-1}^{-1} & \dots & u_{K-1}^{-L} \end{array}\right).$$

Applying the same arguments as in [22], where a similar expression is found for the complex sinusoids in noise, it can be shown that:

$$\boldsymbol{\mathcal{P}_t} \;\; = \;\; \frac{1}{4\pi^2} Re\{\boldsymbol{F}\boldsymbol{G}(\hat{\boldsymbol{a}} - \boldsymbol{a})\} Re\{(\hat{\boldsymbol{a}} - \boldsymbol{a})^T \boldsymbol{G}^T \boldsymbol{F}^T\} = \frac{1}{2} \frac{1}{4\pi^2} Re\{\boldsymbol{F}\boldsymbol{G}\boldsymbol{\mathcal{P}_a}\boldsymbol{G}^H \boldsymbol{F}^H\} \tag{21}$$

where $(\cdot)^H$ denotes Hermitian transpose.

Unfortunately, it appears difficult to derive an explicit expression for the matrix $\boldsymbol{\mathcal{P}_a}$ for the various choices of L, because the vector $\boldsymbol{a}$ changes itself with L. However, it is possible to obtain a compact formula for $\boldsymbol{\mathcal{P}_t}$ that is:

$$\boldsymbol{\mathcal{P}_t} = \frac{1}{2} \frac{1}{4\pi^2} Re\{\boldsymbol{F}\boldsymbol{G}\boldsymbol{H}^\dagger \boldsymbol{\xi}\boldsymbol{\xi}^H \boldsymbol{H}^{\dagger H} \boldsymbol{G}^H \boldsymbol{F}^H\} \tag{22}$$

and investigate the influence of M and L on the estimation accuracy. For the proof of (22) we refer to [12], and its references, where the related problem of estimating sinusoids in noise, is studied.

Now, we show that the order of magnitude of $\boldsymbol{\mathcal{P}}_t$ is $O\left(\frac{1}{R_t^2 R_f^3}\right)$ for sufficiently large M and when L is of the order of M. First, notice that $\boldsymbol{H}$ can be factorized as follows:

$$\begin{aligned}\boldsymbol{H} &= \sum_{k=0}^{K-1} c_k \begin{pmatrix} u_k^{-1} & \dots & u_k^{-L} \\ \vdots & & \vdots \\ u_k^{M} & \dots & u_k^{M-L} \end{pmatrix} \\ &= \begin{pmatrix} 1 & \dots & 1 \\ \vdots & & \vdots \\ u_0^{M} & \dots & u_{K-1}^{M} \end{pmatrix} \begin{pmatrix} c_0 & & 0 \\ & \ddots & \\ 0 & & c_{K-1} \end{pmatrix} \begin{pmatrix} u_0^{-1} & \dots & u_0^{-L} \\ \vdots & & \vdots \\ u_{K-1}^{-1} & \dots & u_{K-1}^{-L} \end{pmatrix} = \boldsymbol{SCG}. \end{aligned} \quad (23)$$

Since all these matrices are of full rank, we can use standard results on the Moore-Penrose pseudoinverse together with (23), to show that:

$$\boldsymbol{H}^{\dagger} = \boldsymbol{G}^H(\boldsymbol{G}\boldsymbol{G}^H)^{-1}\boldsymbol{C}^{-1}(\boldsymbol{S}^H\boldsymbol{S})^{-1}\boldsymbol{S}^H. \quad (24)$$

Inserting (24) in (22) we obtain that:

$$\boldsymbol{\mathcal{P}}_t = \frac{1}{4\pi^2} Re\{\boldsymbol{F}\boldsymbol{C}^{-1}(\boldsymbol{S}^H\boldsymbol{S})^{-1}\boldsymbol{S}^H\boldsymbol{\xi}\boldsymbol{\xi}^H\boldsymbol{S}(\boldsymbol{S}^H\boldsymbol{S})^{-1}\boldsymbol{C}^{-1}\boldsymbol{F}^H\} \quad (25)$$

In the next steps of the proof, we analyze in detail the different terms involving $\boldsymbol{\mathcal{P}}_t$ in (25). We examine the order of each term and use the notation $g = \text{diag}[O(f_1(q))] + O(f_2(q))$ to denote that matrix g has diagonal elements of the order $O(f_1(q))$ and off-diagonal elements of the order $O(f_2(q))$ while $f_1(q)$ and $f_2(q)$ are any two functions of q. For evaluating the order of some terms we also need the following standard result [23] :

$$\frac{1}{M^{s+1}} \sum_{m=1}^{M} m^s e^{-jm(\omega-\overline{\omega})} = \begin{cases} O(1) & \text{for } \omega = \overline{\omega} \text{ and } s \geq 0 \\ O(1/L) - jO(1/L) & \text{for } \omega \neq \overline{\omega} \text{ and } s \geq 0 \end{cases} \quad (26)$$

1) $\boldsymbol{C} = diag[O(1)]$ *and consequently* $\boldsymbol{C}^{-1} = diag[O(1)]$, since $\boldsymbol{C}$ depends only on the signal $x(t)$ and has no dependence on M or L.
2) $\frac{1}{L}\boldsymbol{G}\boldsymbol{G}^H = diag[O(1)] + O(1/L) - jO(1/L)$ *and consequently* $\left(\frac{1}{L}\boldsymbol{G}\boldsymbol{G}^H\right)^{-1} = diag[O(1)] + O(1/L) - jO(1/L)$, which can be verified by direct multiplication using (26).
3) $\frac{1}{M}\boldsymbol{S}^H\boldsymbol{S} = diag[O(1)] + O(1) - jO(1/M)$ *and consequently* $\left(\frac{1}{M}\boldsymbol{S}^H\boldsymbol{S}\right)^{-1} = diag[O(1)] + O(1) - jO(1/M)$, which can be verified again by direct multiplication since the matrix $\boldsymbol{S}$ has a similar structure as $\boldsymbol{G}^H$.
4) $L\boldsymbol{F} = diag[O(1/L) + jO(1)]$ *and consequently* $(L\boldsymbol{F})^{-1} = diag[O(1/L) + jO(1)]$

From the definition of α_k, we have that:

$$\begin{aligned}\frac{1}{L}\alpha_0 &= \frac{1}{L}[\ \cos 2\pi t_0 \quad \cdots \quad L\cos L2\pi t_0\ ]\boldsymbol{A} \\ &= \frac{1}{L}[\ \cos 2\pi t_0 \quad \cdots \quad L\cos L2\pi t_0\ ](-\boldsymbol{H}^{\dagger}\boldsymbol{h}) \\ &= \frac{1}{L^2}[\ \cos 2\pi t_0 \ \cdots \ L\cos L2\pi t_0]\boldsymbol{G}^H\left(\frac{1}{L}\boldsymbol{G}\boldsymbol{G}^H\right)^{-1}\boldsymbol{C}^{-1}\left(\frac{1}{M}\boldsymbol{S}^H\boldsymbol{S}\right)^{-1}\left(\frac{1}{M}\boldsymbol{S}^H\boldsymbol{h}\right). \quad (27)\end{aligned}$$

Next, by multiplying the corresponding matrices, it can also be verified, by direct computation, that:

$$\begin{aligned}&\tfrac{1}{L^2}[\ \cos(2\pi t_0) \quad \cdots \quad L\cos(2L\pi t_0)\ ]\boldsymbol{G}^H = \\ &\qquad = [\ O(1) - jO(1/L) \quad O(1/L) - jO(1/L) \quad \cdots \quad O(1/L) - jO(1/L)\ ].\end{aligned} \quad (28)$$

For the last part in (27) we get that:

$$\frac{1}{M}\boldsymbol{S}^H\boldsymbol{h} = \begin{pmatrix} u_0^0 & \cdots & u_{K-1}^0 \\ \vdots & & \vdots \\ u_0^M & \cdots & u_{K-1}^M \end{pmatrix}^H \begin{pmatrix} \frac{1}{\tau}\sum_{k=0}^{K-1} c_k u_k^0 \\ \vdots \\ \frac{1}{\tau}\sum_{k=0}^{K-1} c_k u_k^M \end{pmatrix} = \frac{1}{M}\begin{pmatrix} \sum_{m=0}^{M}\sum_{k=0}^{K-1} c_k u_k^m u_0^{-m} \\ \vdots \\ \sum_{m=0}^{M}\sum_{k=0}^{K-1} c_k u_k^m u_{K-1}^{-m} \end{pmatrix}.$$

The term on the right hand-side of the previous equation has the following order:

$$\begin{aligned}\frac{1}{M}\sum_{m=0}^{M}\sum_{k=0}^{K-1} c_k u_k^m u_r^{-m} &= \frac{1}{M}\sum_{k=0}^{K-1} c_k + \frac{1}{M}\sum_{m=1}^{M}\sum_{k=0}^{K-1} c_k e^{-j\frac{2\pi}{\tau}m(t_k - t_r)} \\ &= \frac{1}{M}\sum_{k=0}^{K-1} c_k + \frac{1}{M}\sum_{m=1}^{M} c_r + \frac{1}{M}\sum_{m=1}^{M}\sum_{k=0,k\neq r}^{K-1} e^{-j\frac{2\pi}{\tau}m(t_k - t_r)} \\ &= O(1/M) + O(1) + \sum_{k=0,k\neq r}^{K-1} c_k(O(1/M) + jO(1/M)) \\ &= O(1) + jO(1/M)\end{aligned}$$

and therefore

$$\frac{1}{M}\boldsymbol{S}^H\boldsymbol{h} = [O(1) + jO(1/M)]_{K\times 1}. \quad (29)$$

Putting together the results from previous steps and substituting (28) and (29) in (27) and assuming that L and M are of the same order, we can conclude that:

$$\frac{1}{L}\alpha_0 = O(1) + jO(1/L). \quad (30)$$

Similarly:

$$\begin{aligned}&\tfrac{1}{L^2}[\ \sin(2\pi t_0) \quad \cdots \quad L\sin(2L\pi t_0)\ ]\boldsymbol{G}^T = \\ &\qquad = [\ O(1/L) - jO(1) \quad O(1/L) - jO(1/L) \quad \cdots \quad O(1/L) - jO(1/L)\ ],\end{aligned}$$

obtaining for β_0 that:

$$\frac{1}{L}\beta_0 = O(1/L) + jO(1).$$

The same procedure can be used to evaluate the order of $\{\alpha_k, \beta_k\}$ for $k \geq 0$, obtaining:

$$\frac{1}{L}\alpha_k = O(1) + jO(1/L) \quad \text{and} \quad \frac{1}{L}\beta_k = O(1/L) + jO(1).$$

This leads to the conclusion that $L\boldsymbol{F} = \text{diag}[O(1/L) + jO(1)]$.

5) $\boldsymbol{S}^H\boldsymbol{\xi}\boldsymbol{\xi}^H\boldsymbol{S} = MSE(\boldsymbol{X}, \hat{\boldsymbol{X}})O(L) = MSE(\boldsymbol{Y_2}, \hat{\boldsymbol{Y}}_{\boldsymbol{2}})$ *for* $M \geq L$

The key point is that first we can split matrix $\boldsymbol{\xi}\boldsymbol{\xi}^H$ into two terms, one depending only on R_t, and the other one depending only on M and L, or equivalently, on R_f, assuming that L is also of the order of M. Following similar arguments as in [12], the matrix $\boldsymbol{\xi}\boldsymbol{\xi}^H$ can be rewritten as:

$$\boldsymbol{\xi}\boldsymbol{\xi}^H = MSE(\boldsymbol{Y_2}, \hat{\boldsymbol{Y}}_{\boldsymbol{2}})A^*A^T,$$

where $(\cdot)^*$ denotes conjugation of $(\cdot)$ and

$$A = \begin{pmatrix} 1 & a_1 & \cdots & a_L & & 0 \\ & \ddots & \ddots & & \ddots & \\ 0 & & 1 & a_1 & \cdots & a_L \end{pmatrix}_{(M+1|M+L+1)}$$

Thus, it follows that:

$$\boldsymbol{S}^H\boldsymbol{\xi}\boldsymbol{\xi}^H\boldsymbol{S} = MSE(\boldsymbol{Y_2}, \hat{\boldsymbol{Y}}_{\boldsymbol{2}})\boldsymbol{S}^HA^*A^T\boldsymbol{S}.$$

In order to obtain an insight on the order of $\boldsymbol{S}^H\boldsymbol{\xi}\boldsymbol{\xi}^H\boldsymbol{S}$, we compute the explicit form for the case of one Dirac and describe how to generalize the result for the case of K Diracs.

For $K = 1$, we have that:

$$\boldsymbol{S} = \begin{pmatrix} u_0^0 & u_0^1 & \cdots & u_0^M \end{pmatrix}^T, \qquad \boldsymbol{S}^H\boldsymbol{S} = M+1, \qquad \boldsymbol{G}\boldsymbol{G}^H = L,$$

$$\boldsymbol{a} = -\boldsymbol{H}^\dagger c_0 \begin{pmatrix} u_0^0 \\ u_0^1 \\ \vdots \\ u_0^M \end{pmatrix} = -\boldsymbol{G}^H(\boldsymbol{G}\boldsymbol{G}^H)^{-1}\boldsymbol{C}^{-1}(\boldsymbol{S}^H\boldsymbol{S})^{-1}\boldsymbol{S}^H\boldsymbol{S}c_0 = -\frac{1}{L}\begin{pmatrix} u_0^1 \\ \vdots \\ u_0^L \end{pmatrix}$$

Then, for the case where $M \geq L$, we have that:

$$A^T\boldsymbol{S} = \begin{pmatrix} 1 & & \\ -\frac{1}{L}u_0 & & 0 \\ \vdots & \ddots & \\ -\frac{1}{L}u_0^L & & \\ & & 1 \\ & \ddots & -\frac{1}{L}u_0 \\ 0 & & \vdots \\ & & -\frac{1}{L}u_0^L \end{pmatrix} \begin{pmatrix} u_0^0 \\ u_0^1 \\ \vdots \\ u_0^M \end{pmatrix} = \begin{pmatrix} 1 \\ u_0\left(1-\frac{1}{L}\right) \\ \vdots \\ u_0^{L-1}\left(1-\frac{L-1}{L}\right) \\ 0 \\ \vdots \\ 0 \\ -u_0^{M+1}\frac{L}{L} \\ \vdots \\ -u_0^{M+L}\frac{1}{L} \end{pmatrix}$$

and

$$\begin{aligned} \boldsymbol{S}^H A^* A^T \boldsymbol{S} &= 1 + \left(1-\frac{1}{L}\right)^2 + \cdots + \left(1-\frac{L-1}{L}\right)^2 + 1 + \left(\frac{L-1}{L}\right)^2 + \cdots + \left(\frac{1}{L}\right) \\ &= \frac{2}{L^2}\sum_{i=0}^{L} i^2 = \frac{(L+1)(2L+1)}{3L}. \end{aligned}$$

Now, noticing that the coefficients of the annihilating filter have the following form:

$$\boldsymbol{a} = -\boldsymbol{H}^\dagger \boldsymbol{S} \begin{pmatrix} c_0 \\ \vdots \\ c_{K-1} \end{pmatrix} = -(\boldsymbol{G}^H(\boldsymbol{G}\boldsymbol{G}^H)^{-1}\boldsymbol{C}^{-1}(\boldsymbol{S}^H\boldsymbol{S})^{-1}\boldsymbol{S}^H)\boldsymbol{S} \begin{pmatrix} c_0 \\ \vdots \\ c_{K-1} \end{pmatrix} \tag{31}$$

$$= -\boldsymbol{G}^H(\boldsymbol{G}\boldsymbol{G}^H)^{-1} \begin{pmatrix} 1 \\ \vdots \\ 1 \end{pmatrix} = -\frac{1}{L} \begin{pmatrix} \sum_{k=0}^{K-1} u_k^1 + O(1/L) \\ \sum_{k=0}^{K-1} u_k^2 + O(1/L) \\ \vdots \\ \sum_{k=0}^{K-1} u_k^L + O(1/L) \end{pmatrix} \tag{32}$$

then, by doing the same steps as for the case of one Dirac, we get that the diagonal elements of $\boldsymbol{S}^H A^* A^T \boldsymbol{S}$ are of the order O(L), or equivalently:

$$\frac{1}{L}(\cdot)_{ii} = \frac{1}{L}\begin{pmatrix} u_i^0 & u_i^{-1} & \cdots & u_i^{-M} \end{pmatrix} A^* A^T \begin{pmatrix} u_i^0 \\ u_i^1 \\ \vdots \\ u_i^M \end{pmatrix} = O(1) + O(1/L).$$

For the off-diagonal elements, taking into account the specific structure of A^*A^T that follows from (31), we have:

$$|\frac{1}{L}(\cdot)_{ij}| = \left| \frac{1}{L}(\; u_i^0 \quad u_i^{-1} \quad \cdots \quad u_i^{-M} \;) A^*A^T \begin{pmatrix} u_j^0 \\ u_j^1 \\ \vdots \\ u_j^M \end{pmatrix} \right| \leq \frac{1}{L}(\cdot)_{ii} = O(1) + O(1/L).$$

This upper bound is sufficient for us and we do not have to search for tighter bounds. Thus:

$$\boldsymbol{S}^H A^* A^T \boldsymbol{S} = O(L) \tag{33}$$

Finally, we can calculate the order of the matrix $\mathcal{P}_t$ as follows:

$$\begin{aligned} \boldsymbol{\mathcal{P}}_t &= \frac{1}{2}\frac{1}{4\pi^2}\frac{1}{L^2M^2}\mathrm{Re}\left\{ (L\boldsymbol{F})\boldsymbol{C}^{-1}\left(\frac{1}{M}\boldsymbol{S}^T\boldsymbol{S}\right)^{-1}\left(\boldsymbol{S}^T\boldsymbol{\xi}\boldsymbol{\xi}^T\boldsymbol{S}\right)\left(\frac{1}{M}\boldsymbol{S}^T\boldsymbol{S}\right)^{-1}\boldsymbol{C}^{-1}(L\boldsymbol{F})^H \right\} \\ &= \frac{1}{2}\frac{1}{4\pi^2}\frac{L}{L^2M^2}MSE(\boldsymbol{Y_2}, \hat{\boldsymbol{Y}}_{\boldsymbol{2}})[O(1) + jO(1)]_{K\times K} \\ &= \frac{1}{LM^2}d_1(\boldsymbol{y}, \hat{\boldsymbol{y}})[O(1) + jO(1)]_{K\times K} \end{aligned} \tag{34}$$

Changing $L = M = O(R_f)$ in (34) and using the result from Theorem 1 for $\boldsymbol{y} \in \boldsymbol{S_1} \cap \boldsymbol{S_2}$ we get that:

$$\boldsymbol{\mathcal{P}}_t = O\left(\frac{1}{R_t^2 R_f^3}\right).$$

The final results follows from [24], where it is shown that the results derived for the Yule-Walker system and the least square solution has asymptotically the same behavior as the total least square solution. Therefore,

$$d_3(\boldsymbol{y}, \hat{\boldsymbol{y}}) = MSE(\boldsymbol{t}, \hat{\boldsymbol{t}}) = \sum_{i=1}^{K} (\mathcal{P}_t)_{ii} = O\left(\frac{1}{R_t^2 R_f^3}\right). \tag{35}$$

REFERENCES

[1] M. Vetterli, P. Marziliano, and T. Blu, "Sampling signals with finite rate of innovation," IEEE Trans. on Signal Proc., vol. 50, no. 6, pp. 1417–1428, 2002.

[2] I. Maravić and M. Vetterli, "Digital $DS - CDMA$ receiver working below the chip rate: Theory and design," Technical Report IC/2002/018, 2002.

[3] I. Maravić, M. Vetterli, and K. Ramchandran, "High-resolution acquisition methods for wideband communication systems," Proc. of ICASSP, 2003.

[4] P. Ishwar, A. Kumar, and K. Ramchandran, "Distributed sampling for dense sensor networks: a bit-conservation principle," IPSN, 2003.

[5] B. Beferull-Lozano, R. L. Konsbruck, and M. Vetterli, "Rate-distortion problem for physics based distributed sensing," in *Proc. of the Third International Symposium on Information Processing in Sensor Networks (IPSN)*, April 2004.

[6] N. T. Thao and M. Vetterli, "Deterministic analysis of oversampled A/D conversion and decoding improvement based on consistent estimates," Trans. on Signal Proc., vol. 42, no. 3, pp. 519–531, 1994.

[7] B. Beferull-Lozano and A. Ortega, "Efficient quantization for overcomplete expansion in R^N," IEEE Trans. on Information Theory, vol. 49, no. 1, pp. 129–150, 2003.

[8] V. K. Goyal, M. Vetterli, and N. T. Thao, "Quantized overcomplete expansion in R^N: analysis, sinthesis and algorithms," IEEE Trans. on Information Theory, vol. 44, pp. 16–31, 1998.

[9] I. Jovanović and B. Beferull-Lozano, "Oversampled A/D conversion of non-bandlimited signals with finite rate of innovation," in *Proc. of IEEE International Conference on Acoustics, Speech, and Signal Processing*, May 2004.

[10] Z. Cvetković and M. Vetterli, "On simple oversampled A/D conversion in $L^2(\mathcal{R})$," IEEE Trans. on Information Theory, vol. 47, no. 1, pp. 146–154, 2001.

[11] I. Jovanović and B. Beferull-Lozano, "Error-rate dependence of non-bandlimited signals with finite rate of innovation," in *Proc. of IEEE International Symposium on Information Theory (ISIT)*, Chicago, USA, June 2004.

[12] P. Stoica, T. Soderstorm, and F. Ti, "Asymptotic properties of the high-order Yule Walker estimqtes of sinusoidal frequencies," IEEE Trans. on Acus. Speach and Signal Proc., vol. 37, no. 11, pp. 1721–1734, 1989.

[13] S. Van Huffel and J. Vandewalle, *The Total Least Squares Problem: Computational Aspects and Analysis*, vol. 9 of *Frontiers in Applied Mathematics Series*, SIAM, Philadelphia, PA, 1991.

[14] P. Stoica, B. Friedlander, and T. Soderstorm, "A high-order yule-walker method of AR parameters of $ARMA$ model," *Syst. Control Lett.*, vol. 11, pp. 99–105, 1989.

[15] T. K. Moon and W. C. Stirling, *Mathematical Methods and Algorithms for Signal Processing*, Prentice Hall, NJ 07458, 2000.

[16] Z. Cvetković and I. Daubechies, "Single-bit oversampled A/D conversion with exponential accuracy in the bit-rate," in *Data Compression Conference (DCC)*, Snowbird, Utah, 2000.

[17] Z. Cvetković, "Resilience properties of redundant expansions under additive noise and quantization," IEEE Trans. on Information Theory, vol. 49, no. 3, pp. 644–656, 2003.

[18] Z. Cvetković, "Source coding with quantized redundant expansions: Accuracy and reconstruction," in *Data Compression Conference (DCC)*, Snowbird, Utah, 1999.

[19] N. T. Thao and M. Vetterli, "Reduction of the MSE in r-times oversampled A/D conversion from $O(1/r)$ to $O(1/r^2)$," IEEE Trans. on Signal Proc., vol. 42, no. 1, pp. 200–203, 1994.

[20] R. J. Duffin and A. C. Schaeffer, "A class of nonharmonic fourier series," *Trans. Amer. Math. Soc.*, vol. 72, pp. 341–366, 1952.

[21] H. J. Landau, "Sampling, data transmission, and the Nyquist rate," *Proc.* IEEE, vol. 55, pp. 200–2003, 1994.

[22] T. Soderstorm and P. Stoica, "Accuracy of high-order Yule-Walker methods for frequency estimation of complex sine waves," *IEE Proceedings-F*, vol. 140, no. 1, pp. 71–80, 1993.

[23] I. S. Gradshteyn and I. M. Ryzhik, *Table of Integrals, Series and Products*, New York: Academic, 1980.

[24] P. Stoica, T. Soderstorm, and S. Van Huffel, "On SVD-based and TLS-based high-order Yule-Walker methods for frequency estimation," *Signal Processing*, vol. 29, pp. 309–317, 1992.